Morphological Transformation of Shock Waves Behind a Flat Plate

Se-Myong Chang[*†]
BK21 Contract Professor, Seoul National University
Soogab Lee
Associate Professor, Seoul National University
Keun-Shik Chang
Professor, Korea Advanced Institute of Science and Technology

The interaction of a travelling shock with the shear layer of a flat plate is studied computationally. The Euler and Navier-Stokes equations are solved numerically on quadrilateral unstructured adaptive grids. The flat plate is installed horizontally on the central axis of a shock tube. The shear layer is first created by two shock waves at different speeds splitted by a flat plate. A series of small vortices is developed as a consequence in the shear layer. The shock wave reflected at the end wall impinges the shear layer. The complicated shock dynamics in the evolution to the pseudo-steady state is represented with the morphological transformation of a planar shock into an oblique shock.

Key Words : Shock-Vortex Interaction, Shear Layer, Compressible Vortex, TVD Method, Quadrilateral Unstructured Adaptive Grid

1. Introduction

The interaction of a shock-driven flow and a slipstream of a supersonic jet has been regarded as the primary source of screech-tone acoustic waves that are critical for aircraft noises in aerospace engineering. Basic study on shock-vortexlet interaction will give us the proper understanding of a simpler model in the viewpoint of flow physics. The planar moving shock wave interacting with the shear layer downstream of a jet nozzle converges nearly to a steady state in only a few milliseconds, but the gap between the two states still remains to be hidden as a mystery.

The earlier researchers, Dosanjh and Weeks (1965), experimentally visualized the interaction of a straight travelling shock wave and a Karman vortex street behind a cylinder, but the extreme complexity of the multiple-vortex model producing a turbulent wake made it difficult to comprehend the essential physics. As computational techniques are developed, primary attention is focased on more fundamental problems like a shock and single vortex interaction in terms of proper numerical models (Meadows et.al., 1991; Ellzey et.al., 1995; chatterjee, 1999). In their studies it was been elucidated that the shock-vortex interaction generates the deformation of a shock wave as well as the quadrupolar radiation of acoustic waves.

The argument in this paper is motivated by the previous studies on shock-shear layer interaction and shock-vortex interaction. A simpler model than Dosanjh and Weeks(1965) based on a practical experiment is introduced to restrain turbulence in a given time scale. A plane shock wave impinges successive multiple small vortices produced by Kelvin-Helmholtz instability along a

† First Author
* Corresponding Author,
E-mail : smc1972@dreamwiz.com
TEL : +82-2-880-1902; **FAX** : +82-2-887-2662
BK21 contract professor, seoul National University, San 56-1, Shinlim-dong, Kwanak-ku, Seoul 151-742, Korea.
(Manuscript **Received** August 21, 2000 ; **Revised** February 12, 2001)

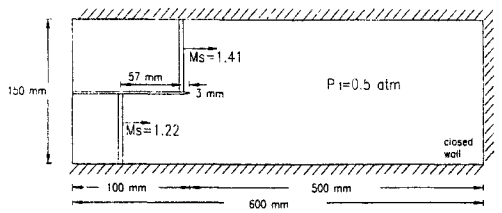

Fig. 1 Definition of the present problem

linear shear layer bounded by two fluid regions of difference velocities. The Euler and Navier-Stokes equations are solved numerically on quadrilateral unstructured adaptive grids to achieve effectively the sufficient resolution for morphological shock wave transformation.

2. Problem Definition

Figure 1 shows the computational domain and the initial condition for this problem. It is based on a shock tube experiment (Chang, 2000) with the driven-section pressure set egual to $p_1=0.5$ atm. The driver gas is air ($\gamma=1.4$). The faster shock, $M_s=1.41$ (above the flat plate) starts 57 mm ahead of the slower shock, $M_s=1.22$ (below the flat plate). The flat plate with 1mm thickness has its aft tip sharply polished and aligned to the flow direction.

The unsteady Euler and Navier-Stokes equations are solved numerically. No-slip boundary conditions are applied on the walls for the Navier-Stokes equations while flow tangency conditions are employed for the Euler equations. A non-reflecting boundary condition is applied at the left inlet of Fig. 1 (Hirsch, 1990).

3. Brief Description of the Numerical Algorithm

A TVD high-resolution method is used to solve the Euler and Navier Stokes equations with the boundary conditions For more accurate and efficient computations, we introduced a quadrilateral unstructured adaptive grid (QUAG) system (de Zeeuw and Powell, 1993; Ko and Chang, 1998).

3.1 TVD high-resolution method

Finite-volume integral equations are derived from the differential form of the Euler and Navier-Stokes equations. The spatial fluxes of convective terms are simply discretized by applying the Gaussian divergence theorem. According to the Roe flux-difference scheme to obtain approximate solutions of the Riemann problem, the right-bounded numerical flux of a cell is expressed as a combination of eigenvectors (Roe, 1981). We take a central difference, for the viscous flux, while the viscous flux is set to zero in the Euler equations.

To obtain second-order accuracy, MUSCL (Monotone Upstream-centered Schemes for Conservative Laws) algorithm is used with the van Leer slope limiter (Hirsch, 1990). We can obtain the instantaneous flow field at every time step by the explicit time marching.

3.2 Quadrilateral unstructured adaptive grid

Generally, quadrilateral grids have some advantages over triangular grids widely used in computational fluid dynamics. They show less skewness and better quality for a simple geometry. Unstructured grid system can be created and treated easily except for its complicated connectivity. Besides, the adaptive grid may reduce the computing load without degrading the resolution around stiff-gradient regions.

The error indicator of a cell is defined as the sum of density or velocity differences (Chang and Chang, 1999). We use the density-based error indicator for Euler equations as

$$\varepsilon_e=\sum_{j=1}^{4}\left|\rho_e-\rho_{C_j(e)}\right| \tag{1}$$

The velocity-based error indicator for Navier-Stokes equations is

$$\varepsilon_e=\sum_{j=1}^{4}\sqrt{\sum_{i=1}^{2}(u_{ie}-u_{iC_j(e)})^2} \tag{2}$$

where e is the cell index and $C_j(e)$ denotes the neighbor cell in the j direction. A cell is divided into four equal subcells when the indicator in Eqs. (1)-(2) exceeds a preset criterion. A reverse action is taken when the error falls below the

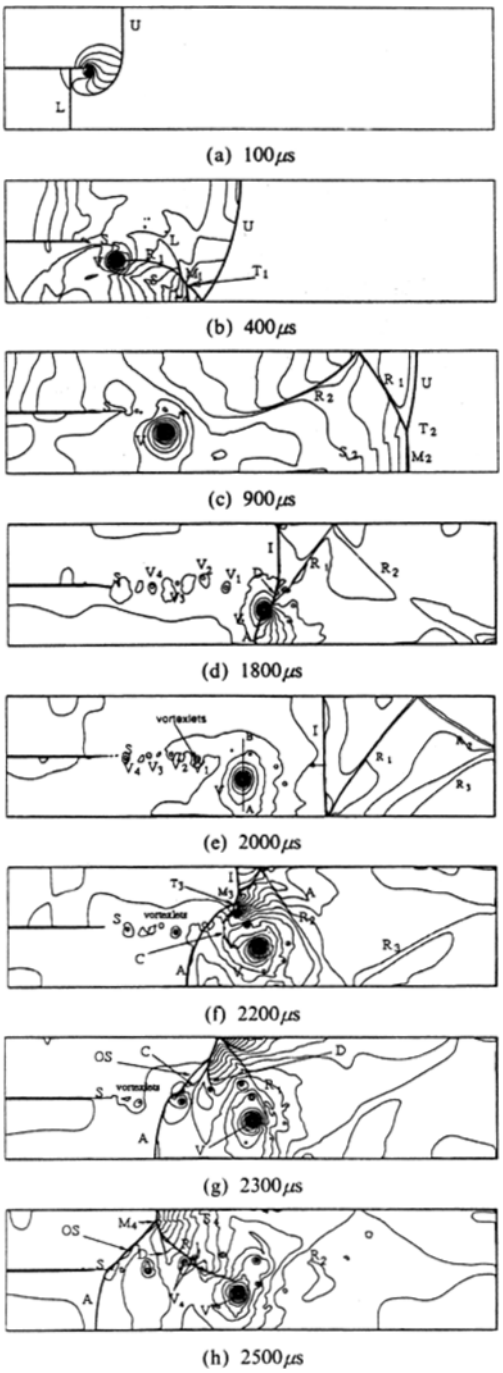

Fig. 2 Numerical simulation: Navier-Stokes solution

criterion. This refinement/unrefinement procedure is repeated four to seven levels in every time step during time integration. In comparison with common structured grids, the unstructured grids need more computer memory to store the data sets of linked list and quadtree recording connectivity of cells and refinement levels.

4. Result and Discussion

Some representative constant density contours or the isopycnics are plotted in Fig. 2(a)-(h), the solution of Navier-Stokes equations. A constant wall temperature is assumed, and the adaptive level is set to five.

The entire flow regime is divided into two stages: Fig. 2(a)-(c) are Stage 1, and Fig. 2(d)-(h) are Stage 2, as classified by the authors. The two fluid layers at different velocities separated by the flat plate are mixed in a curvilinear shear layer: see Fig. 2(a)-(c). Multiple vorticities on the shear layer are developed due to Kelvin-Helmholtz instability. The travelling shock is reflected back from the end wall of the shock tube in Fig. 2(d). It produces successive shock-vortex interactions: see Fig. 2(e)-(h).

4.1 On the overall physics

The upper shock (U) at $M_s=1.41$ arrives at the trailing edge of the flat plate ahead of the lower shock (L) at $M_s=1.22$. In Fig. 2(a), U is diffracted to produce a starting vortex (V) fed by the shear layer (S) whereas L is yet to arrive at the trailing edge. Figure 2(b) shows a shock-shock interaction between the lower shock (L) and the reflected shock (R_1) of U, making a piece of Mach stem (M_1) between the two triple points (T_1's). The two shocks L and R_1 interact with V in sequence. In Fig. 2(c), R_1 is reflected from the upper wall to a secondary reflected shock (R_2). U and R_1 make a triple point (T_2) and a new Mach stem (M_2) with a slip line (S_2) emanating from T_2. As U is propagated downstream, M_2 is extended to the original shape of a plane shock (I) in Fig. 2(d). The reflected shock R_1, R_2, and R_3 are all parasitic waves, not directly related with the present discussion.

The vortex (V) is rotating in the clockwise direction. Therefore, the shock I is deformed by the vortex with the accelerated wave (A) and the decelerated shock (D) (sivier, et al., 1992). The wave A is accelerated to a circular form and it is in interaction with D to make a third Mach stem (M_3) connected to the triple points (T_3's): see Fig. 2(f). In Fig. 2(f)-(g), the shock D interacts with the multiple vortices in the shear layer to produce a compressive wave such as C. The wave C is attached to the wave A. It eventually merges with A to form an oblique shock (OS) in Fig. 2(h).

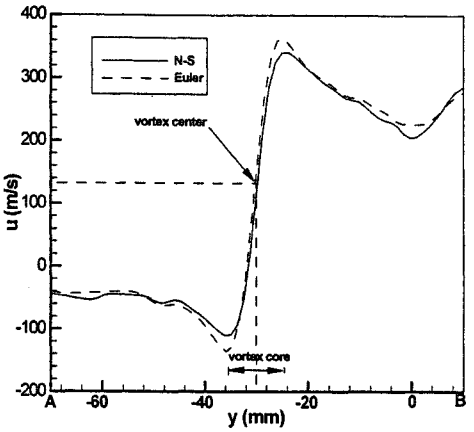

(a) Tangential velocity

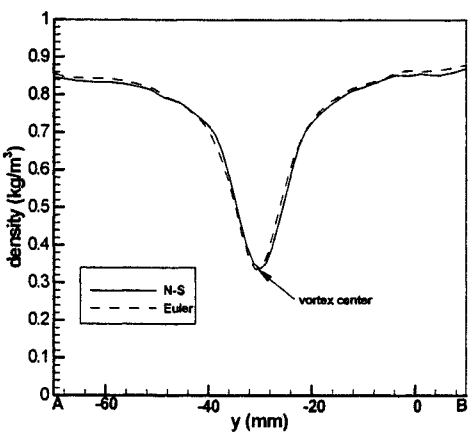

(b) Density profile

Fig. 3 Vortex structure

4.2 Structure and motion of the vortex

In Fig. 3(a) for tangential velocity, the Euler simulation predicts the shear layer (the boundary of rotational vortex core and outer potential flow) more sharply than the Navier-Stokes simulation. However, this difference is hardly found in Fig. 3 (b) for density profile. The qualitative structure is not much changed between inviscid and viscous simulations: see also the vortex trajectories in Fig. 4. The diffusion terms in the Navier-Stokes

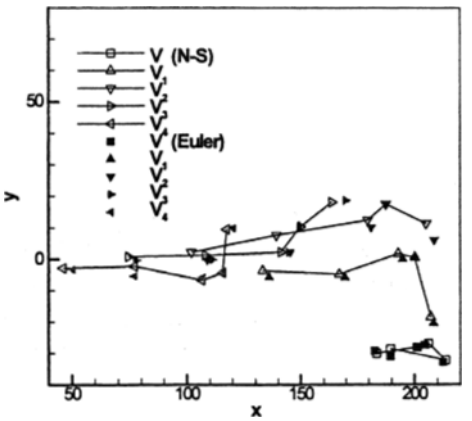

Fig. 4 Vortex motion

equations play the role of dissipation, which is very small during a short time scale.

The vortex structure is investigated by velocity (u_1) and density (ρ) distributions along the vertical line, AB, through the instantaneous center of main vortex in Fig. 3(a)-(b). The line AB at $x=$ 190 mm are marked in Fig. 2(d). In the Cartesian coordinate system, $x=0$ is defined at the trailing edge of the splitter plate. The dashed lines are from the Euler solution and the solid lines are from the Navier-Stokes solution. The flow region is cleanly divided into the solid-rotating vortex core and the outer field. Density is the minimum at the vortex core. At the peek velocity in Fig. 3 (a), the difference between the two simulations contains a relative error about 15 %.

The discernable vortices are numbered V_1, V_2, $\cdots$ in Fig. 2(d), and Fig. 4 is the trajectory of their centers. At first, they are deflected vertically by the incident shock (I), and sequentially sucked into the main vortex. It is observed that the shock wave even can split a vortex: see Fig. 2(h) where the shock R_1 splits V_4 into two subvortices: only the bigger left one is traced in Fig. 4.

4.3 Morphological transformation of shock waves

The returning shock (I) heads into the small multiple vortices in the shear layer of the flat plate in Fig. 2(e)-(h). As a result of successive interactions with the vortices, an envelope of the strong compression wave (C) is produced: see

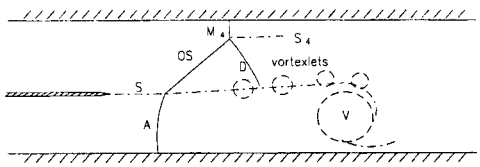

Fig. 5 Final stage of the morphological transformation

Fig. 2(g). This wave C merges with the preceding shock to form a fortified oblique shock (OS) in Fig. 2(h).

The instantaneous streamlines near the two-fluid boundary are parallel to the slip stream (S), which we call the shear layer. It conceptually has a finite thickness in the viscous model. Owing to the clockwise motion of the vortices, the shear layer is lifted up in the downstream direction to form a ramp when viewed from the observer drifting at the shock speed. Although the head wind from the inlet above the flat plate is subsonic, its relative velocity in the shock-fixed frame is supersonic. It is becauce the OS is moving upstream with

$$M_i = M_{inlet} + M_{OS}\sin\theta_i \tag{3}$$

Here, M_i is the relative flow Mach number, M_{inlet} is the inlet head-wind Mach number, M_{OS} is the shock Mach number of OS, and θ_i is the incident angle of OS to the inlet flow. In Fig. 2(h), using the flow data $M_{inlet}=0.66$, $M_{OS}=0.68$, and $\theta_1=42.3°$, the relative flow Mach number becomes $M_i=1.12$ (supersonic) according to Eq. (3). $M_i>1$ or $M_i<1$ is an important criterion related with temporal stability of a moving shock wave. When it is supersonic, the oblique shock (OS) will propagate preserving its shape. Otherwise, the shock will turn to fade out. A shock can exist even in subsonic field, althoagh it needs a supersonic relative velocity by the fundamental rule in gas dynamics.

In Fig. 5, a schematic sketch is drawn for the shock and shear layer interaction. The oblique shock (OS) originates from the ramp-like shear layer, or slip line (S) and reflected from the upper wall to make a Mach stem (M_4) and a slip line (S_4). We can also identify these waves in Fig. 2 (h). The process of the morphological

transformation from the shocks U and L in Fig. 2 (a) is completed resulting in the shocks OS and A.

5. Concluding Remarks

The interaction of a shock wave and multiple vortices has not been modeled clearly since the experimental investigation in 1965(Dosanjh and Weeks). The short time scale (~2.5 msec) in the present model allow us to avoid turbulence in a shock tube, so investigation on the morphological transformation of shock waves become more feasible. The dimensional analysis on the time scale can be found in Chang(2000). The finite-volume Euler and Navier-Stokes code based on the TVD high-resolution method and the quadrilateral unstructured adaptive grid system is adopted to solve the present problem.

Successive interaction of the incident shock and multiple small vortices first produces a compressive wave (C) which is merged into the preceding shock wave (OS): see Fig. 2(g)-(h). The shear layer parallel to the streamline of the mixing jet forms a ramp due to the vortex motion while the new oblique shock (OS) in the pseudo -steady state is generated. At the initial state of Stage 2, Fig. 2(d), the shock I collides successively with the vortices V, V_1, V_2, ···. At the final state, Fig. 2(h), the new shock OS and its reflections (R_1 and M_4) are generated by the morphological transformation.

One of our primary question is "How much important is the viscosity in such problems ? ". We conclude that viscosity cannot change the flow and the wave structure without turbulence although the effect may be noticed qualitatively in Fig. 3(a), for example.

Acknowledgement

This work was supported by the Brain Korea 21 Project in 2001.

Reference

Chang, S.M., 2000, "Unsteady Shock Wave-Vortex Interactions in the Compressible Shear Layer," Ph. D. Thesis, Korea Advanced Institute of Science and Technology.

Chang, S.M. and Chang K.S., 1999, "Weak Shock Reflection from a Blunt Body," *Transaction of KSME (B)*, Vol. 23, pp. 901~910.

Chang, S.M. and Chang K.S., 2000, "On the Shock-Vortex Interaction in Schardin's Problem," *Shock Waves*, Vol. 10, pp. 333~343.

Chang S.M. and Chang K.S., 2000, "Visualization of Shock-Vortex Interaction Radiating Acoustic Waves," *Journal of Visualization, Visualization Society of Japan*, Vol. 3, pp. 221~228.

Chatterjee, A., 1999, "Shock Wave Deformation in Shock-Vortex Interactions," *Shock Waves*, Vol. 9, pp. 95~105.

Dosanjh, D.S., and Weeks, T.M., 1965, "Interaction of a Starting Vortex as Well as a Vortex Street with a Travelling Shock Wave," *AIAA Journal*, Vol. 3, pp. 216~223.

Ellzey, J.L., Henneke M.R., Picone J.M., Oran E.S., 1995, "The Interaction of a Shock Wave with a Vortex: Shock Distortion and the Production of Acoustic Waves," *Physics of Fluids*, Vol. 7, pp. 172~184.

Hirsch, C., 1990, *Numerical Computation of Internal and External Flows*, John Wiley.

Ko, S.M., Chang K.S., 1998, "Resonant Pulsatile Flows of a Hartmann-Sprenger Tube," *CFD Journal*, Vol. 6, pp. 439~452.

Meadows, K.R., Kumar A, Hussaini M.Y., 1991, "Computational Study on the Interaction Between a Vortex and a Shock Wave," *AIAA Journal*, Vol. 29, pp. 174~179.

Roe, P.L. 1981, "Approximate Riemann Solvers, Parameter Vectors and Difference Schemes," *Journal of Computational Physics*, Vol. 43, pp. 357~372,.

Sivier, S., Loth E., Baum J., Lohner R., 1992, "Vorticity Produced by Shock Wave Diffraction," *Shock Waves*, Vol. 2, pp. 31~41.

de Zeeuw, D., Powell K.G., 1993, "An Adaptive Refined Cartesian Mesh Solver for the Euler Equations," *Journal of Computational Physics*, Vol. 104, pp. 56~68.